Monthly Notices
of the
ROYAL ASTRONOMICAL SOCIETY

MNRAS **469,** 2737–2749 (2017)
Advance Access publication 2017 May 1

doi:10.1093/mnras/stx1039

The limits of cosmic shear

Thomas D. Kitching,[1⋆] Justin Alsing,[2,3] Alan F. Heavens,[2] Raul Jimenez,[4,5] Jason D. McEwen[1] and Licia Verde[4,5]

[1]*Mullard Space Science Laboratory, University College London, Holmbury St Mary, Dorking, Surrey RH5 6NT, UK*
[2]*ICIC, Astrophysics, Imperial College, Blackett Laboratory, Prince Consort Road, London SW7 2AZ, UK*
[3]*Center for Computational Astrophysics, 160 5th Ave, New York, NY 10010, USA*
[4]*ICC, University of Barcelona, IEEC-UB, Marti Franques, 1, E-08028 Barcelona, Spain*
[5]*ICREA, Pg. Lluis Companys 23, E-08010 Barcelona, Spain*

Accepted 2017 April 27. Received 2017 April 19; in original form 2016 November 15

ABSTRACT

In this paper, we discuss the commonly used limiting cases, or approximations, for two-point cosmic-shear statistics. We discuss the most prominent assumptions in this statistic: the flat-sky (small angle limit), the Limber (Bessel-to-delta function limit) and the Hankel transform (large ℓ-mode limit) approximations; that the vast majority of cosmic-shear results to date have used simultaneously. We find that the combined effect of these approximations can suppress power by $\gtrsim 1$ per cent on scales of $\ell \lesssim 40$. A fully non-approximated cosmic-shear study should use a spherical-sky, non-Limber-approximated power spectrum analysis and a transform involving Wigner small-d matrices in place of the Hankel transform. These effects, unaccounted for, would constitute at least 11 per cent of the total budget for systematic effects for a power spectrum analysis of a *Euclid*-like experiment; but they are unnecessary.

Key words: large-scale structure of Universe – cosmology: theory.

1 INTRODUCTION

Weak lensing is the phenomenon whereby the images of distant galaxies are distorted by the effect of gravitational potentials caused by matter perturbations along the line of sight. This gravitational lensing effect induces a small change in the ellipticity[1] of a galaxy's image known as shear. The shear caused by the large-scale structure of the Universe is known as 'cosmic shear'. The mean of the complex cosmic-shear field is zero but its two-point correlation function or power spectrum contains cosmological information; cosmic shear is also used as a synonym for this statistic. This statistic is a particularly sensitive probe of dark energy because it measures the power spectrum of matter overdensity perturbations across large portions of the expansion history of the Universe. Because of this, there are several on-going wide-field surveys that attempt to measure this effect, for example, CFHTLenS (Heymans et al. 2012), DES (The DES Collaboration 2015), DLS (Jee et al. 2016), KiDS (Kuijken et al. 2015) and HyperSuprimeCam; as well as several more planned surveys, for example, *Euclid*[2] (Laureijs et al. 2011), LSST (Tyson et al. 2003) and *WFIRST* (National Research Council 2010), that have the measurement of this statistic as one of their primary science goals.

In practice, there are several ways in which the cosmic-shear two-point statistic can be computed that can be broadly categorized into real/configuration-space measurements as a function of celestial angle (e.g. shear correlation functions), and angular spherical-harmonic/Fourier-space measurements (e.g. power spectra). Furthermore, these statistics can be computed in a series of redshift bins, to capture the geometry of the three-dimensional (3D) shear field, an approach known as 'tomography'; or a spherical-Bessel/Fourier-space measurement in the radial direction known as 'three-dimensional' cosmic shear (Heavens 2003; Castro, Heavens & Kitching 2005; Kitching et al. 2007).

In this paper, we present each of the primary approximations in cosmic-shear statistics and explicitly link all of the currently used statistics together into a general schema. In doing so, we also present a general 3D spherical-radial statistic, which is the redshift-space equivalent of a spherical-Bessel analysis. We discuss various approximations and a data compression, namely: flat-sky, Limber, tomography and Hankel transformations. The flat-sky assumption projects on to a locally flat tangent plane on the sky. The tomographic data compression, presented in Hu (1999), is a lossy binning of the cosmic-shear signal into several redshift bins and is an approach used by *all* cosmic-shear studies (see Kilbinger 2015 for a review) except those that use a spherical-Bessel representation (e.g. Kitching et al. 2014), for both theoretical studies and data analysis. In Kitching, Heavens & Miller (2011) and Kitching et al. (2014) it was shown how to derive the tomographic case from a more general spherical-Bessel representation of the shear field. The Limber approximation links angular and radial wavenumbers together via a comoving distance relation. This was first discussed in Kaiser (1998) in the context of cosmic shear and has been investigated in

⋆ E-mail: t.kitching@ucl.ac.uk
[1] Third flattening, or third eccentricity.
[2] http://euclid-ec.org

Kitching et al. (2011) in cosmic-shear studies, but in the majority of theoretical studies and data analyses it is an assumption. There is a particularly clear illustration of the Limber approximation in LoVerde & Afshordi (2008) that we discuss in this paper.

Most of the approximations we investigate are used simultaneously and in combination. Notably, all the primary cosmological results from all of the wide-field surveys use a flat-sky, tomographic, Limber-approximated correlation function analysis, e.g. Heymans et al. (2013) for CFHTLenS; The DES Collaboration (2015) for DES; Jee et al. (2016), and Hildebrandt et al. (2017) for KiDS. Notable exceptions include Pen, Van Waerbeke & Mellier (2002), Brown et al. (2003), Heymans et al. (2005), Köhlinger et al. (2016), Alsing, Heavens & Jaffe (2017) and the `PolSpice` measurements in The DES Collaboration (2015), all whom used Fourier-space measurements in angle, with the flat-sky, tomographic and Limber approximations. In Kitching et al. (2007, 2014) a flat-sky spherical-Bessel analysis was used without the tomographic or Limber approximations.

This paper is presented in the following manner. In Section 2, we review the cosmic-shear formalism starting with the spherical-Bessel representation and then present the spherical-radial and correlation function representations. In Section 3, we discuss the flat-sky, tomographic and Limber approximations and present a general schema for linking these statistics and approximations. We discuss the implications of this for current results in Section 4. We discuss conclusions in Section 5.

2 COSMIC-SHEAR METHODS

We begin by introducing several versions of the two-point cosmic-shear statistic that treat the data, and represent the underlying 3D shear field, in different ways. The first of these is the spherical-Bessel representation that has been described in detail in Heavens (2003), Castro et al. (2005), Heavens, Kitching & Taylor (2006), Kitching, Taylor & Heavens (2008) and Kitching et al. (2011, 2007, 2014), the second is the presentation of a spherical-radial representation of which the commonly used tomographic statistic (Hu 1999) is a simple approximation. We then discuss real/configuration-space representations.

2.1 The spherical-Bessel representation

The cosmic-shear field has spin-weight 2, and we can perform a spherical-Bessel transform to obtain

$$\gamma_\ell^m(k) = \left(\frac{2}{\pi}\right)^{1/2} \sum_g \gamma_g(r_g, \theta_g) j_\ell(k r_g) {}_2Y_\ell^m(\theta_g) \tag{1}$$

where the sum is over all galaxies g at 3D comoving coordinates (r_g, θ_g), k is a radial wavenumber and ℓ is an angular wavenumber. The $j(kr_g)$ are spherical-Bessel functions. The ${}_2Y_\ell^m(\theta_g)$ are spin-weight 2 spherical harmonics. Such a sum can be used to construct the data vector for a spherical-Bessel analysis of weak-lensing data, which is then compared with the following theoretical covariance, as described in Kitching et al. (2014). When applying this sum to data, these transformed coefficients can be manipulated to extract the pure E- and B-mode signals (where cosmic shear is only expected to produce an E-mode signal), and remove any multiplicative measurement biases (where the measured γ_g is related to the true $\gamma_g^{\rm T}$ via some linear relation $\gamma_g = (1+m)\gamma^{\rm T}$, where m is an estimated bias parameter) as described in Kitching et al. (2014). The sum over galaxies is an estimator for a continuous integral over angle and radius, where there is an additional shot-noise contribution to the covariance, due to having a finite number of galaxies at discrete points (see Heavens 2003). The factor $(2/\pi)^{1/2}$ is a convention that is consistent with Heavens et al. (2006; equation 2).

The mean of equation (1) is zero, but the covariance of the transform coefficients is non-zero. Assuming isotropy, the covariance of the harmonic coefficients – known as the power spectrum – can be written as

$$\langle \gamma_\ell^m(k) \gamma_{\ell'}^{m'*}(k') \rangle = C_\ell^{\rm SB}(k, k') \delta_{\ell\ell'} \delta_{mm'}. \tag{2}$$

Using the notation of Kitching et al. (2011), we can write down the theoretical expectation value of the power spectrum for given a cosmology

$$C_\ell^{\rm SB}(k, k') = |D_\ell|^2 \mathcal{A}^2 \left(\frac{2}{\pi}\right) \int \frac{{\rm d}\tilde{k}}{\tilde{k}^2} G_\ell^{\rm SB}(k, \tilde{k}) G_\ell^{\rm SB}(k', \tilde{k}), \tag{3}$$

where the pre-factor $\mathcal{A} = 3\Omega_{\rm M} H_0^2/(2c^2)$ (where H_0 is the current value of the Hubble parameter, $\Omega_{\rm M}$ is the ratio of the total matter density to the critical density and c is the speed of light in a vacuum). The variable $|D_\ell| = \sqrt{(\ell+2)!/(\ell-2)!}$ in the spherical case (see Castro et al. 2005; and Leistedt et al. 2015). The temptation in the flat-sky case is to approximate $|D_\ell| = \ell^2$, but this is an approximation. The G matrix is given by

$$G_\ell^{\rm SB}(k, \tilde{k}) = \int {\rm d}z_{\rm p}\, j_\ell(k r(z_{\rm p})) n(z_{\rm p}) \times \int {\rm d}z'\, p(z'|z_{\rm p}) U_\ell(r[z'], \tilde{k}), \tag{4}$$

where $n(z_{\rm p})\,{\rm d}z_{\rm p}$ is the number of galaxies in a spherical shell of radius $z_{\rm p}$ and thickness ${\rm d}z_{\rm p}$ and $p(z'|z_{\rm p})$ is the probability of a galaxy with photometric redshift $z_{\rm p}$ having a true redshift z'. The U matrix is given by

$$U_\ell(r[z], k) = \int_0^{r[z]} {\rm d}r' \frac{F_K(r, r')}{a(r')} j_\ell(k r') P^{1/2}(k, r'), \tag{5}$$

where $P(k, r[z])$ is the matter power spectrum at comoving distance $r[z]$ and radial wavenumber k. The comoving distance r is used to express the time dependence of the power spectrum; we could equally use t as a label, or $r(t)$. $F_K = S_K(r - r')/S_K(r)/S_K(r')$ is the 'lensing kernel' where $S_K(r) = \sinh(r)$, r, $\sin(r)$ for cosmologies with spatial curvature $K = -1$, 0, 1, and $a(r)$ is the dimensionless scalefactor at the cosmic time related to the look-back time at comoving distance r. Note that already we have made an approximation, in that the statistics strictly depend on unequal-time correlators (Kitching & Heavens 2017), but we will not discuss this point further here.

2.2 The spherical-radial representation

A different way to represent the 3D shear field is to make a Fourier-like decomposition in angular wavenumber but *not* in the radial direction. This decomposition is the following

$$\gamma_\ell^m(z) = \left(\frac{2}{\pi}\right)^{1/2} \sum_{g \in z} \gamma_g(r_g, \theta_g) {}_2Y_\ell^m(\theta_g) \tag{6}$$

which is still a 3D representation of the data, except that it excludes the radial-Bessel transform. The sum in this case is over all galaxies that have a redshift z. We refer to this as the 'spherical-radial' transform (as opposed to a spherical-Bessel transform).

Again the mean of this representation is zero, but the covariance is non-zero. Using the notation above, we can write down the

theoretical expectation value of the power spectrum given a cosmology

$$C_\ell^{\rm SR}(z,z') = |D_\ell|^2 \mathcal{A}^2 \left(\frac{2}{\pi}\right) \int \frac{{\rm d}k}{k^2} G_\ell^{\rm SR}(z,k) G_\ell^{\rm SR}(z',k), \quad (7)$$

where in this case the $G^{\rm SR}$ matrix is given by

$$G_\ell^{\rm SR}(z,k) = \int {\rm d}z_{\rm p} W^{\rm SR}(z,z_{\rm p}) n(z_{\rm p}) \times \int {\rm d}z' p(z'|z_{\rm p}) U_\ell(r[z'],k), \quad (8)$$

where $W(z, z_{\rm p})$ is a redshift-dependent weight function that defines the 'bin-width' in redshift over which the statistic is defined for redshift z. The U matrices are the same as in equation (5). In the case that $W^{\rm SR}(z, z_{\rm p}) = \delta^D(z - z_{\rm p})$, this covariance is still a complete representation of the shear field when z and z' span $[0, \infty)$.

2.3 The configuration-space representation

As an alternative to performing a cosmic-shear statistic in Fourier/Bessel space, the analysis can be done in real/angular/configuration space, where instead of an angular wavenumber, an angle θ is used on the celestial sphere as the dependent variable. Such statistics are readily computed from data by summing over pairs of galaxies (see e.g. Kilbinger 2015). From theory, these are related to the cosmic-shear power spectra through a transform that results in two correlation functions that we derive in Appendix A:

$$\xi_+(\theta,z,z') = \frac{1}{2\pi}\sum_\ell (\ell+0.5) d^\ell_{22}(\theta) \times \left[C_\ell^{\rm SR,E}(z,z') + C_\ell^{\rm SR,B}(z,z')\right]$$
$$\xi_-(\theta,z,z') = \frac{1}{2\pi}\sum_\ell (\ell+0.5) d^\ell_{-22}(\theta) \times \left[C_\ell^{\rm SR,E}(z,z') - C_\ell^{\rm SR,B}(z,z')\right], \quad (9)$$

where d^ℓ_{22} and d^ℓ_{-22} are Wigner small-d matrices.[3] θ are angular separations on the sphere. This can be derived in a number of ways either starting from Hu (2000, Appendix A), from the results of Ng & Liu (1999), or from considering the additive properties of the Wigner large-D matrices. In this case, the power spectra in the integrals are a combinations of both E-mode and B-mode components; however, from theory, the B-mode is typically always zero. Note that, the spin nature of the field must be considered in relating the power spectra to the correlation functions and it should not be treated as a scalar field.

2.3.1 *Large Wavenumber Limit*

In the limit that $\ell \gg |m|, |m'|$ (in the cosmic-shear case $|\ell| \gg 2$), the Wigner-d matrices can be written as Bessel functions of the first kind, which is what has been done in cosmic-shear studies to date. Making the further approximation that $\ell \simeq \ell + 0.5$, the transforms in equation (9) are commonly assumed to be Hankel transforms:

$$\xi_+(\theta,z,z') = \frac{1}{2\pi}\sum_\ell \ell J_0(\ell\theta) \times \left[C_\ell^{\rm SR,E}(z,z') + C_\ell^{\rm SR,B}(z,z')\right]$$
$$\xi_-(\theta,z,z') = \frac{1}{2\pi}\sum_\ell \ell J_4(\ell\theta) \times \left[C_\ell^{\rm SR,E}(z,z') - C_\ell^{\rm SR,B}(z,z')\right]. \quad (10)$$

Hankel transforms can be performed using either a 3D power spectrum, as we have used here, or on tomographically binned data. An inverse-Hankel transform can also be defined as, for example, $C_\ell^{\rm SR}(z,z') = \int {\rm d}\theta\theta J_0(\ell\theta)\xi_+(\theta,z,z')$, but since this formally requires an integration over *all* angles, it is not well defined in a flat-sky case.

In the cosmic-shear representations that are based on spherical harmonic transforms, the angular wavenumbers can be approximately related to celestial angular separations through $\theta = \pi/\ell$. However, after performing the Hankel transformation, the relationship between the angle θ in equations (10) is more complicated. To investigate this relation, we plot in Fig. 1, the Bessel function amplitudes in equation (10) as a function of ℓ mode and θ, for the ξ_+ and ξ_- functions. It is clear from these figures that every angle samples from all ℓ modes but weighted in a different way. To estimate which ℓ modes contribute to the Hankel transform integrals, we compute the following integrals over θ

$$\mathcal{W}_+(\ell,z,z') = \int_{\theta_{\rm min}}^{\theta_{\rm max}} {\rm d}\theta \left[\ell J_0(\ell\theta) C_\ell^{\rm SR}(z,z')\right],$$
$$\mathcal{W}_-(\ell,z,z') = \int_{\theta_{\rm min}}^{\theta_{\rm max}} {\rm d}\theta \left[\ell J_0(\ell\theta) C_\ell^{\rm SR}(z,z')\right]. \quad (11)$$

These are the weight functions in ℓ mode, integrated over all angles, that are applicable for analyses that require a sum over angle (such as a likelihood function). We use $\theta_{\rm max} = 100$ arcmin, and vary $\theta_{\rm min}$ and show these functions in Fig. 1. To compute the maximum ℓ mode to minimum θ relationship, we compute the cumulative functions

$$\left(\frac{1}{A}\right) \int_2^{\ell_{\rm max}} {\rm d}\ell \, |\mathcal{W}_+(\ell,r,r')| = f \leq 1, \quad (12)$$

which we calculate as a discrete sum, where $A = \int_2^\infty {\rm d}\ell \, |\mathcal{W}_+(\ell,r,r')|$. These functions converge to machine precision only at $\ell_{\rm max} \to \infty$, so in practice, a tolerance needs to be defined, f, where it is considered that most of the information is captured. We set this to $f = 0.995$, i.e. 99.5 per cent of the integral content is captured by this limit; we find that setting a limit larger than this results in numerical errors becoming dominant. We plot this derived $\ell_{\rm max}$ in Fig. 1, and find that the link between $\ell_{\rm max}$ and $\theta_{\rm min}$ is well approximated by the following scaling functions:

$$\xi_+ : \log_{10}[\ell_{\rm max}] = -0.14 \log_{10}(\theta_{\rm min}/{\rm arcmin}) + 4.06,$$
$$\xi_- : \log_{10}[\ell_{\rm max}] = -0.19 \log_{10}(\theta_{\rm min}/{\rm arcmin}) + 4.49. \quad (13)$$

We find that the ξ_- statistic is much more sensitive to high-ℓ modes than ξ_+. For typical minimum angles used in data analysis of $\theta_{\rm min} \sim 0.1$ arcmin, we find that the maximum wavenumber probed is approximately $\ell_{\rm max} \sim 5 \times 10^4$ for the ξ_+ statistic, but the bulk of the signal comes from $\ell < 1000$.

Finally, there are several ways of filtering the 'raw' correlation function measurement (equation 10) that have been proposed for example Top-hat statistics, Map statistics (e.g. Munshi, Valageas & Barber 2004) and COSEBIs (e.g. Schneider, Eifler & Krause 2010). The motivation for these, and their mathematical detail, are well summarized and reviewed in Kilbinger (2015).

[3] We provide tabulated values of these here http://goo.gl/UUQIUx.

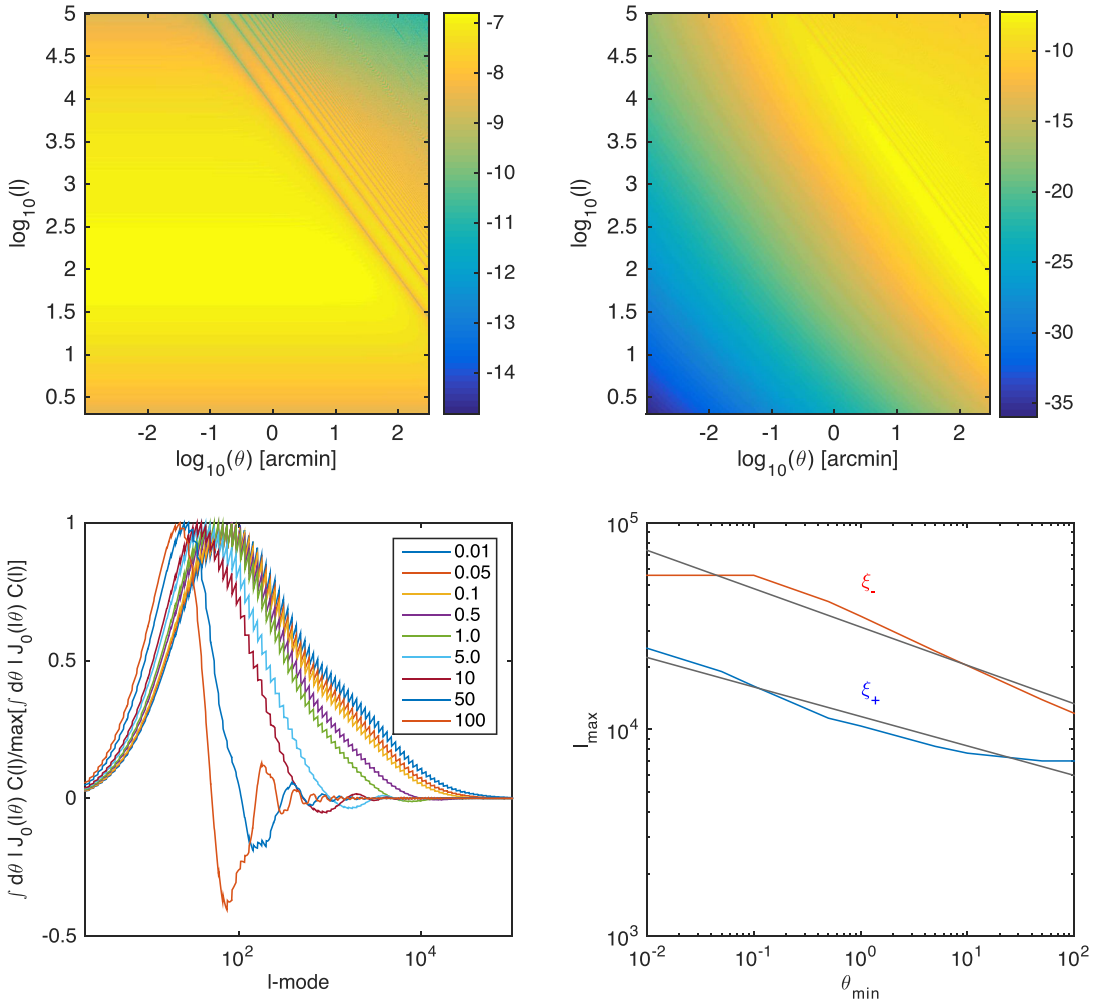

Figure 1. The top panels show the functions $\ell J_0(\ell\theta)C_\ell^{\rm SR}(z,z)$ (left-hand panel) and $\ell J_4(\ell\theta)C_\ell^{\rm SR}(z,z)$ (right-hand panel) for an auto-correlation cosmic-shear power spectrum $C_\ell^{\rm SR}(z,z)$ evaluated at a redshift of zero; although we find results in this figure are insensitive to this assumption. The colour scales denote the logarithm (base 10) of the magnitude of the functions that correspond to the ξ_+ and ξ_- Hankel transforms (equation 10), respectively. The lower left-hand panel shows the normalized integral $\int {\rm d}\theta \ell J_0(\ell\theta)C_\ell^M(z,z)$ over θ to show the integrated weighting of $\int {\rm d}\theta \xi_\pm(\theta)$ as a function of ℓ modes for a variety of angular ranges $\theta_{\rm min} \leq \theta\,{\rm arcmin}^{-1} \leq 100$. The different labelled colours in this plot show different $\theta_{\rm min}$ in arcmin. The lower right-hand panel shows the $\ell_{\rm max}$ where these integrals converge as a function of $\theta_{\rm min}$ for the ξ_+ (blue) and ξ_- (red) Hankel transforms. The fitted functions in equation (13) are shown in grey.

3 COSMIC-SHEAR APPROXIMATIONS

We will now investigate the impact of several approximations that are commonly used in cosmic-shear studies. We will address the flat-sky and Limber approximations, but will not discuss source-source clustering (Schneider, Van Waerbeke & Mellier 2002), source-lens clustering (Bernardeau 1998; Hamana et al. 2002), the Born approximation (Cooray & Hu 2002), higher order power spectrum terms (Krause & Hirata 2010) or unequal-time correlators (Kitching & Heavens 2017); all of which are expected to have an effect for future surveys (*Euclid*, LSST and *WFIRST*) but not for current surveys.

3.1 The flat-sky approximation

The flat-sky approximation assumes that the angular extent of the observational field is small and hence the geometry of the angular component is assumed to be planar (i.e. Euclidean). In this case, a planar transform is done instead of a spherical transform in equations (1) and (6), which results in an exponential term $\exp(i\boldsymbol{\ell}\cdot\theta)$ instead of the spin spherical harmonics.

In the case of computing the transform coefficients from data, equations (1) and (6), this results in a different sum over galaxies. In the computation of data vectors, the weighting as a function of ℓ mode is therefore significantly different (see e.g. Hu 2000).

However, in the computation of the theoretical covariances, due to the similar orthogonality relations between both the spherical harmonic and the exponential functions, equations (3) and (7), this only results in a simple change to the pre-factor $|D_\ell|$ from $|D_\ell| = \sqrt{(\ell+2)!/(\ell-2)!} \rightarrow \ell^2$. This is a result of the different ways that the spin raising and lowering operators (that relate the shear field to the gravitational potential field) act on the spin spherical harmonics and the exponential functions; see appendix A of Castro et al. (2005). The impact of this approximation on the amplitude of the cosmic-shear covariance can then very simply be computed. It is a poor approximation as it introduces errors of order $1/\ell$, which may not be negligible.

We note that taking a small angle approximation of the spherical harmonics (see Castro et al. 2005 Section V; or Varshalovich, Moskalev, & Khersonskiĭ 1988 for more complete expressions) results in much larger differences in the amplitude of the power spectra

than that captured in the change of local derivative of the lens potential, but this case has not been considered in the cosmic-shear literature to date.

3.2 Tomographic data compression

The tomographic approximation involves the computation of projected 2D power spectra in a series of redshift bins including the inter-bin (auto-correlation) and intra-bin (cross-correlation) power spectra. This is not an approximation in itself, but it is a lossy data compression.

We look at the effect of this binning by first relating the spherical-Bessel and spherical-radial transforms together. As shown in Kitching et al. (2014), the shear transform coefficients, from our equations (1) and (6), can be related through a radial transform

$$\gamma_\ell^m(z_1) = \int \mathrm{d}r\, W^{\rm SR}[z_1, z(r)] \int \mathrm{d}k j_\ell(kr)\gamma_\ell^m(k), \tag{14}$$

where the weight function is the same one that appears in equation (8), where the integrand of comoving distance r is related to a redshift $z(r)$, and describes the bins as a function of redshift. When referring to tomography, we use numbered redshifts, for example, z_1 and z_2, rather than z and z'. We note that only in the case that the weight function is a delta-function is this a full description of the 3D shear field. In the case that the bin-width is finite, we will refer to this as a 'tomographic' representation of the shear field.

By taking the covariance of equation (14), the two power spectra can be related through

$$\begin{aligned} C_\ell^{\rm SR}(z_1, z_2) = & \int \mathrm{d}k\mathrm{d}k'\mathrm{d}r'\mathrm{d}r'' \\ & \times W^{\rm SR}[z_1, z(r')]W^{\rm SR}[z_2, z(r'')] \\ & \times j_\ell(kr')j_\ell(k'r'')C_\ell^{\rm SB}(k, k'). \end{aligned} \tag{15}$$

This transformation from spherical-Bessel to spherical-radial (tomographic) representations can be performed for any integrable weight function $W^{\rm SR}$; this is also discussed in Castro et al. (2005).

The reverse transform can also be computed, but *only* in the case that the weight function is a delta-function in redshift. In this specific case, the reverse transform is

$$C_\ell^{\rm SB}(k, k') = \int \mathrm{d}z\mathrm{d}z'\, j_\ell(kr[z])j_\ell(k'r[z'])C_\ell^{\rm SR}(z_1, z_2), \tag{16}$$

where the integration over redshift is formally over $0 \leq z < \infty$.

It has been shown (e.g. Bridle & King 2007) that, because of intrinsic alignments, 10–20 redshift bins are required in order for the cosmic-shear power spectrum to be sufficiently sampled in redshift to extract the majority of cosmological information. This is because the lensing kernel is a relatively broad function in redshift space. This is applicable when describing the shear field using the spherical-radial representation, with the caveats that such current studies of the convergence of this approximation have assumed the flat-sky and Limber approximations (that we discuss in the next Section).

3.3 The Limber approximation

The Limber (Limber 1953) approximation was first introduced in Kaiser (1998) for cosmic-shear studies as a method for rendering the calculations more tractable and understandable, and has subsequently been used in the majority of the cosmic-shear studies, both in methodological development and in applications to data. In LoVerde & Afshordi (2008), a particularly clear explanation of the approximation was provided. This assumed that the matter power spectrum was not evolving, i.e. it can be expressed as a function of k-mode only $P(k)$ (LoVerde & Afshordi 2008; equation 5). Unfortunately, the LoVerde & Afshordi (2008) approximation is not directly appropriate at all orders for the cosmic-shear setting where the shear field is an integrated effect over an evolving matter power spectrum; an assumption that we address in Appendix B. In Kitching et al. (2011), the effect of the Limber approximation on cosmic shear was investigated using the LoVerde & Afshordi (2008) approximation, and an effect on the expected error bars of cosmological parameters was predicted.

If the Limber approximation is assumed then using the Kaiser (1998) and LoVerde & Afshordi (2008) approximation, the spherical-radial representation of the cosmic-shear field can be written as

$$C_\ell^{\rm SR}(z_1, z_2) \simeq |D_\ell|^2\mathcal{A}^2 \int \frac{\mathrm{d}k}{k^2} P(k, \nu/k)f(z_1, \nu, k)f(z_2, \nu, k), \tag{17}$$

where the variable $\nu = \ell + 1/2$. In Appendix B, we show that this is indeed the first order approximation to the cosmic-shear power spectrum despite the assumption of a constant matter power spectrum; however, the expansion of this to higher order results in a convergence towards the unapproximated case only if redshift-independent limits in angular wavenumber are assumed. The kernel functions are

$$\begin{aligned} f(z_1, \nu, k) = & \left(\frac{1}{\nu k^2}\right)^{1/2} \int \mathrm{d}z'\mathrm{d}z_{\rm p} n(z_{\rm p})p(z'|z_{\rm p})W^{\rm SR}(z_1, z_{\rm p}) \\ & \times \frac{F_K(r[z'], \nu/k)}{a(\nu/k)}. \end{aligned} \tag{18}$$

This expression is not entirely in the same form as commonly used in the cosmic-shear literature (e.g. Hu 1999; Joachimi & Bridle 2010; Heymans et al. 2013), where the standard form is to use an inner integral over r instead of k mode. As shown in Appendix B, when doing this, we find that the Limber-approximated power is given by

$$C_\ell^{\rm SR,L}(z_1, z_2) \simeq |D_\ell|^2\mathcal{A}^2 \left(\frac{1}{\nu^4}\right) \int \mathrm{d}r \frac{q(r_1, r)q(r_2, r)}{r^2} P(\nu/r, r), \tag{19}$$

where

$$\begin{aligned} q(r_1, r) = & \frac{r}{a(r)} \int \mathrm{d}z_{\rm p}\mathrm{d}z' n(z_{\rm p})p(z'|z_{\rm p})W^{\rm SR}(z_1, z_{\rm p}) \\ & \times \left(\frac{r(z') - r}{r(z')}\right), \end{aligned} \tag{20}$$

where we have expanded the function F_K, and we have assumed here a flat-geometry ($K = 0$). This is the standard form for the cosmic-shear power spectrum (see e.g. Hu 1999; Joachimi & Bridle 2010), except that there is an ℓ-dependent pre-factor

$$T_\ell = \frac{|D_\ell|^2}{\nu^4} = \frac{(\ell + 2)(\ell + 1)\ell(\ell - 1)}{(\ell + 0.5)^4}. \tag{21}$$

T_ℓ is normally replaced by 1. One justification for this is to replace the numerator by ℓ^4 in the flat-sky approximation, and to take a high-ℓ approximation $\nu \simeq \ell$ in the denominator. Note that, a flat-sky approximation that also retains the Limber ν^{-4} dependence would lead to an inaccurate T_ℓ, which differs from unity at $\mathcal{O}(1/\ell)$, and leads to significant errors at low ℓ. Note that, T_ℓ differs from unity only at $\mathcal{O}(1/\ell^2)$, so the standard approximation is good for current data, but there is no reason at all not to use the full expression.

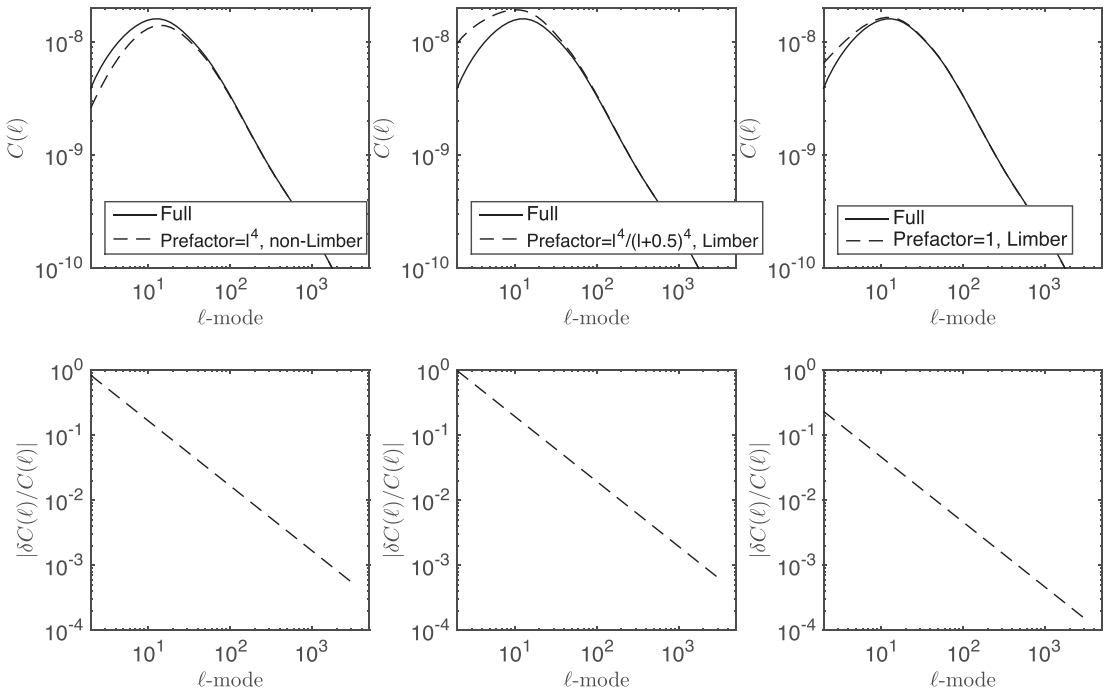

Figure 2. Top panels: The solid line is the full $C(\ell)$ cosmic-shear power spectrum, for a CFHTLenS $n(z)$; not assuming any of the approximations listed in Section 3.4 i.e. flat-sky, Limber, pre-factor-unity or integral variable assumptions. In the full case, the ℓ-dependent pre-factor to the power spectrum is $(\ell+2)!/(\ell-2)!$ and the Limber approximation is not assumed. The dashed lines show the power spectrum when each of the approximations is applied in combination in the panels from left- to right-hand side, the ℓ expressions denote the power spectrum pre-factor used. The lower panels show the modulus of the fractional difference between the full case and the approximated cases $|[C^{\rm Full}(\ell)-C^{\rm Approx}(\ell)]/C^{\rm Full}(\ell)|$.

Up to first order, the Limber approximation can be summarized by comparing equation (7) with equation (17) as a replacement of Bessel functions with scaled delta functions inside the integrals

$$j_\ell(kr) \rightarrow \sqrt{\frac{\pi}{2\ell+1}}\delta^D(\ell+1/2-kr). \tag{22}$$

This expression shows how the Limber approximation acts to link the angular and radial modes through the relation $\ell = kr[z]-1/2$, that we also derive in Appendix B, which has an important effect on the computation of cosmic-shear power spectra.

3.4 The impact of the approximations

There are various steps in the derivation of a configuration-space shear statistic, which involve relating the lensing potential power spectrum on the (spherical) sky to the matter power spectrum, then computing the shear power spectrum on the sky and from there transforming into configuration space if desired. These steps can introduce approximations beyond the Born approximation and approximations of unequal-time correlators, but some are not necessary. At the first stage, it may be necessary to use the Limber approximation for computational tractability reasons. At low ℓ, this is a poor approximation, and if speed is an issue, the next term in the Limber approximation (LoVerde & Afshordi 2008) should be considered. In moving from lensing potential to shear, the full ℓ-dependent pre-factor of $(\ell+2)(\ell+1)\ell(\ell-1)$ should be included, and not approximated by the flat-sky ℓ^4 value. If the Limber approximation is used, $\ell+1/2$ should not be approximated by ℓ. Finally, in computing configuration-space quantities such as shear correlation functions, finite sums over ℓ should be done, using Wigner small-d matrices (equation 9), and not approximated by Hankel transforms.

In summary, in going from the full cosmic-shear expressions to those that are commonly used, there are a series of approximations. These are, starting from a spherical-sky non-Limber-approximated power spectrum, as follows:

(i) Flat-sky approximation: The assumption of a flat-sky changes the pre-factor in the shear–shear power spectrum from $(\ell+2)(\ell+1)\ell(\ell-1)$ to ℓ^4. This is inaccurate and unnecessary.

(ii) Limber approximation: The first-order Limber approximation involves changing the Bessel functions to scaled delta functions using equation (22), leading to a pre-factor in the shear power spectrum of $(\ell+2)(\ell+1)\ell(\ell-1)/(\ell+0.5)^4$.

(iii) Pre-factor unity approximation: In the Limber function expression, a further approximation can be made that the ℓ-dependent pre-factor is unity i.e. $T_\ell = 1$ in equation (21). This is good to $\mathcal{O}(1/\ell^2)$, but is unnecessary.

(iv) Integral variable approximation: In the Limber approximation, the inner variable $\ell+0.5$ is sometimes replaced by ℓ in the argument to the matter power spectrum. This is inaccurate and unnecessary and is not used in this paper.

(v) Hankel-transform approximation: Then when transforming into real-space, a Hankel transform can be used instead of a spherical sky correlation function (equation 9). This leads to an increasing error with angle, and a spherical summation over ℓ modes is preferred.

Each of these approximations acts independently, the first four act on the cosmic-shear power spectrum, and the last only in the case that this is transformed into real-space.

3.4.1 Impact on the power spectrum

In Fig. 2, we show the impact of the flat-sky, Limber and pre-factor-unity approximations. Throughout, we do not make the integral variable approximation, and use a cosmology equal

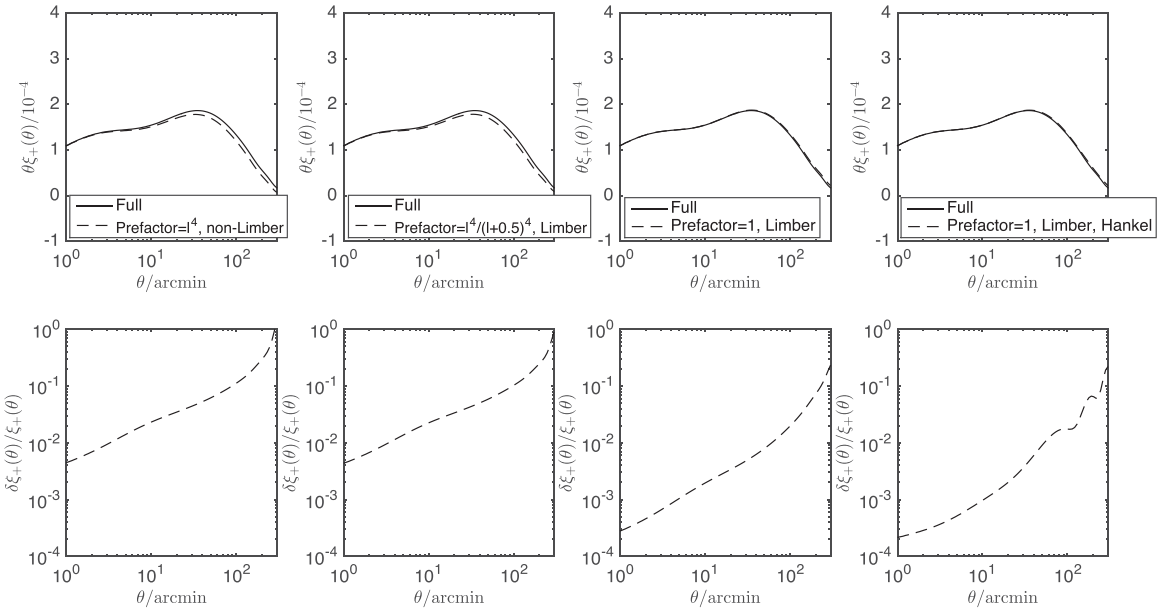

Figure 3. Top panels: The solid line is the full projected $\xi_+(\theta)$ cosmic-shear correlation function, for a CFHTLenS $n(z)$; not assuming any of the approximations listed in Section 3.4 i.e. flat-sky, Limber, pre-factor-unity, integral variable or Hankel assumptions. In the full case, the ℓ-dependent pre-factor to the power spectrum is $(\ell+2)!/(\ell-2)!$, the Limber approximation is not assumed, and a transform using Wigner small-d matrices (equation 9) is used. The dashed lines show the correlation function when each of the approximations is applied in combination in the panels from the left- to right-hand side. The lower panels show the modulus of the fractional different between the full case and the approximated cases $|[\xi_+^{\rm Full}(\theta) - \xi_+^{\rm Approx}(\theta)]/\xi_+^{\rm Full}(\theta)|$.

to the Planck Collaboration I (2016, table 4 TT+low P) best-fitting values. It can be seen that for $\ell \lesssim 10$, there is a more than 10 per cent suppression in the power due to the flat-sky approximation, which reduces to $\lesssim 1$ per cent for $\ell \gtrsim 100$. We can assess the impact of these approximations by computing the integrated effect over the differences

$$\langle \mathcal{A} \rangle / N_A = \frac{\int {\rm d}\ln\ell\, \ell^2 \delta C(\ell)}{\int {\rm d}\ln\ell\, \ell^2}; \tag{23}$$

complementary formulations are provided for this quantity in Massey et al. (2013), Cropper et al. (2013) and Amara & Réfrégier (2008); here, we include a normalization $N_A = \int {\rm d}\ln\ell\, \ell^2$ as suggested by Massey et al. (2013). In general, a non-zero $\langle \mathcal{A} \rangle$ will change the amplitude of the power spectrum and bias cosmological parameter inference. As discussed in Massey et al. (2013), the requirement on the amplitude of this quantity is $\langle \mathcal{A} \rangle / N_A \leq 1.8 \times 10^{-12}$ for a *Euclid*- or LSST-like weak-lensing survey to return unbiased results on the dark energy equation of state parameters, this requirement is an allowance for *all* systematic effects including instrumental and algorithmic quantities. We find that for the best approximated case to the full power spectrum (where the pre-factor is unity and the Limber approximation is assumed) $\langle \mathcal{A} \rangle / N_A = 1.9 \times 10^{-13}$, which would account for 11 per cent of the total budget for systematic effects for a *Euclid* or LSST-like experiment that suggests such approximations should not be used. If scales of $\ell < 100$ are ignored then we find only a modest change with $\langle \mathcal{A} \rangle / N_A = 1.7 \times 10^{-13}$ (note the ℓ^2 factor in equation 23 that gives higher weight to larger ℓ modes).

3.4.2 Impact on the correlation functions

In Figs 3 and 4, we show the impact of the successive approximations on the real-space correlation functions.

Similarly to the power spectrum investigations, we find that the flat-sky approximation on its own has a large effect, but that again the assumption of a unity pre-factor cancels out the approximation changes somewhat. In general, we find that these low-ℓ approximations have a more significant impact on ξ_+ than ξ_-, as may be expected from Section 2.3. The additional step of assuming a Hankel transform rather than a transform that uses Wigner small-d matrices (equation 10 instead of equation 9) results in only a small additional change at scales greater than 10 arcmin; we show only this effect in Fig. 5.

There are currently no explicit requirements set on the correlation function amplitude changes in the literature for future experiments that we are aware of, so it is not possible to assess the applicability of these requirements for *Euclid*-like experiments. However, we note that percent to tens of percent-level changes can occur and, given that the full case is not particularly more computationally demanding than the approximate cases, we recommend that the full case is used.

3.5 A schema of cosmic-shear statistics

Each of the cosmic-shear representations and approximations can be linked in a series of transformations that relate one to the other. For example in Kitching et al. (2011) and Kitching et al. (2014), we show how to relate the spherical-Bessel to the tomographic representation (we also show this in Appendix B). In this paper, we show how to transform from the spherical-Bessel into spherical-radial cases. The flat-sky and configuration-space approximations are well-known as we have discussed.

We show how all of these are linked together in Fig. 4, where we relate each of the cosmic-shear statistics together via the network of approximations that can be employed. In this figure, arrows indicate the direction that the transform takes the statistic, where only one

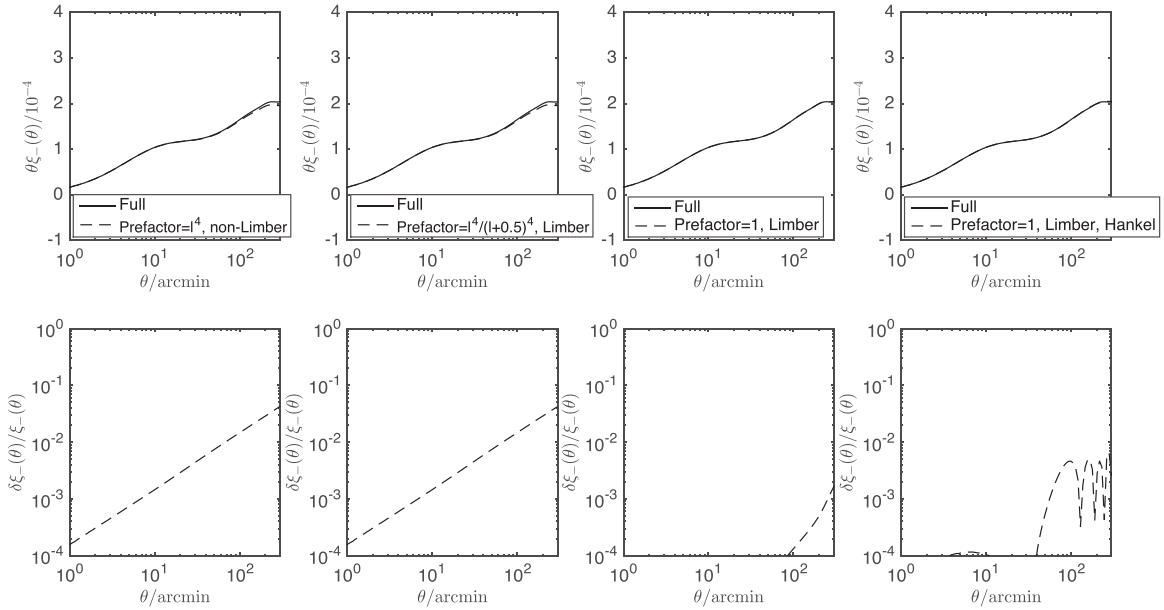

Figure 4. Top panels: The solid line is the full projected $\xi_-(\theta)$ cosmic-shear correlation function, for a CFHTLenS $n(z)$; not assuming any of the approximations listed in Section 3.4 i.e. flat-sky, Limber, pre-factor-unity, integral variable or Hankel assumptions. In the full case, the ℓ-dependent pre-factor to the power spectrum is $(\ell+2)!/(\ell-2)!$, the Limber approximation is not assumed, and a transform using Wigner small-d matrices (equation 9) is used. The dashed lines show the correlation function when each of the approximations is applied in combination in the panels from left- to right-hand side. The lower panels show the modulus of the fractional different between the full case and the approximated cases $|[\xi_-^{\rm Full}(\theta) - \xi_-^{\rm Approx}(\theta)]/\xi_-^{\rm Full}(\theta)|$.

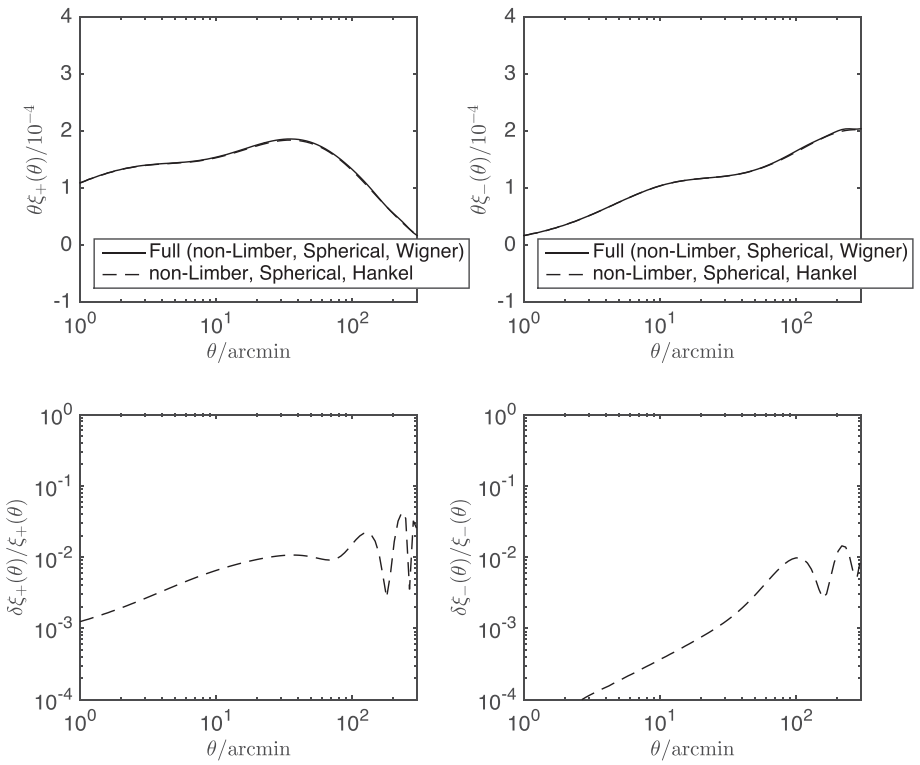

Figure 5. Top panels: The solid line is the full projected $\xi_{+/-}(\theta)$ cosmic-shear correlation function, for a CFHTLenS $n(z)$; not assuming any of the approximations listed in Section 3.4 i.e. flat-sky, Limber, pre-factor-unity, integral variable or Hankel assumptions. The dashed lines show the power spectrum when the Hankel transform instead of the full Wigner-d expression is used. The lower panels show the modulus of the fractional different between the full case and the approximated cases.

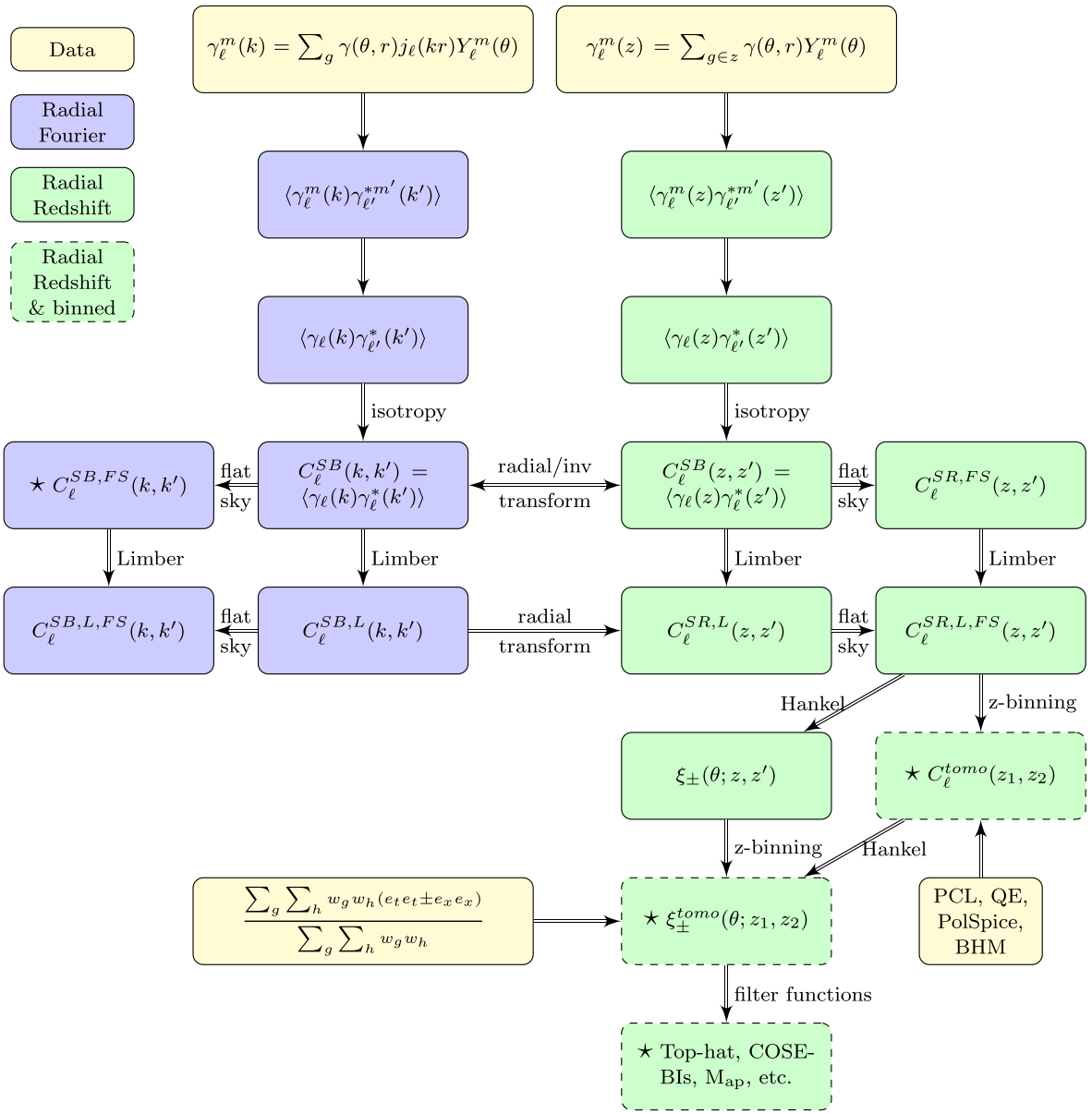

Figure 6. A schema relating each cosmic-shear approximation to all others. For brevity, we do not include spherical-sky or non-Limber-approximated Hankel-like transforms (defined in Castro et al. 2005, Section V) as these are not currently in use. Each arrow shows the direction in which a functional approximation or change is applied where the majority of approximations are irreversible. The yellow boxes show places where a statistic can, and has been approximated from data; these are a direct spherical-Bessel transform (top), a direct correlation function estimator (left-hand panel), and several power spectrum estimators that are Pseudo-$C(\ell)$ (e.g. Hikage et al. 2011), Quadratic Estimator (Hu & White 2001), Polspice (The DES Collaboration 2015) and Bayesian Hierarchical Modelling (BHM, e.g. Alsing et al. 2016, 2017). The blue boxes show statistics that treat the radial (redshift) direction using a Fourier-like/spherical-Bessel analysis, the green boxes show statistics that treat the radial direction directly in redshift space. The solid framed boxes denote full 3D statistics and the dashed framed boxes show redshift binned or 'tomographic' statistics. The superscript acronyms SB, SR, FS and L refer to spherical-Bessel, spherical-radial, flat-sky and Limber approximations, respectively. Isotropy refers to angular isotropy but not radial, as the shear field probes different look-back times in the expansion history. The labels (k, k') and (z, z') denote continuous scale and redshift variables, and (z_1, z_2) to discretized redshifts. The lower box denoting filter functions refers to Map (e.g. Munshi et al. 2004), COSEBI (Schneider et al. 2010) and top-hat statistics. The stars '$\star$' show which statistics have been applied to data.

such case is reversible[4] (the 3D radial transform). We also link the points at which estimators from data are linked to the theoretical statistics, and highlight those statistics that have been applied to data. This provides a visual way to understand what transformation needs to be made to interpret any given cosmic-shear data analysis, where any statistical assumptions have been made, and how a given observation can be translated into another.

[4] By reversible we mean that it can be performed in either direction, without loss of information.

4 DISCUSSION

There have been several other investigations into the Limber approximation. For example Giannantonio et al. (2012) concluded that the Limber approximation is accurate for $\ell \gtrsim 20$. However,

Giannantonio et al. (2012), equations 25 and 26, neglect a factor of $(\ell + 2)!/(\ell - 2)!$ (or l^4 in the flat-sky limit), and also use k^2 in the inner integral (β in their notation) not $(1/k^2)$ (which is the appropriate factor for the cosmic-shear case).

Jeong, Komatsu & Jain (2009) tested the effect of the Limber approximation on the convergence–convergence power spectra and found a $\sim$1 per cent change in power at $\ell \lesssim 100$, and a 10 per cent change at scales $\ell \lesssim 10$. This result is partly consistent with our analysis where a 10 per cent change in the amplitude of the $C_\ell^{\rm SR}(z, z')$ shear–shear power spectrum at $\ell \sim 10$ would propagate into ξ_+ and ξ_- statistics with a similar decrease in power on the real-space angular scales presented in current data analyses. However, the range of k modes and redshift ranges is not quoted in that paper (in particular if a $kr < \ell$ limit is imposed or not), which makes a detailed comparison difficult. Simon (2007) performed a similar study of the Limber approximation in the galaxy clustering context and found that there is a $\sim$10 per cent bias in the correlation function at scales of $\theta \simeq 260$ arcmin. Bernardeau et al. (2012) show that the Limber-approximated power spectrum is accurate to better than 1 per cent at $\ell > 8$; however, their non-Limber approximated expression uses the primordial Newtonian potential power spectrum $P(k)$ that is non-evolving (see their equation 45 where the power spectrum is taken out of the integrations over comoving distance).

Kitching et al. (2011) applied the LoVerde & Afshordi (2008) approximation (equation 22) in the spherical-Bessel case and compared the case of full (k, z) integration with the $\ell > kr$ case, and found a $<$10 per cent change in the amplitude of $C_\ell^{\rm SB}(k, k')$ using the Limber approximation, which was approximately constant as a function of ℓ mode, which is consistent with the results found in this paper. Including the first and second order corrections suggested by LoVerde & Afshordi (2008) are likely to reduce the impact further at low-ℓ modes.

Power spectrum methods, that measure the cosmic-shear two-point statistics as a function of ℓ mode, are more immune to these approximations than correlation function methods because removing $\ell \lesssim 100$ from an analysis will eliminate most of the low-ℓ mode effects. This is the approach taken in Köhlinger et al. (2016) and Alsing et al. (2017) (both of which made the flat-sky, Limber and tomographic approximations). However, power spectrum methods that use a pseudo-$C(l)$, or a mixing matrix method, to account for real-space masks will also encounter additional complexity if the masks mix low-ℓ modes and higher ℓ-modes (e.g. Hikage et al. 2011). Finally, super-sample covariance (Takada & Hu 2013) that causes correlations between the power spectrum errors across ℓ modes will also mix low-ℓ and high-ℓ behaviour.

5 CONCLUSION

In this paper, we present the spherical-Bessel and spherical-radial representations of cosmic shear, and discuss the correlation function representation. We discuss several approximations and limits of these statistics including the flat-sky, tomographic and Limber approximations. Whilst, the tomographic approximation is expected to be relatively benign – because the lensing kernel is relatively smooth in redshift – the flat-sky and Limber approximations change the statistical behaviour of the cosmic-shear statistic at large scales. We also find a subtlety in the derivation of the standard Limber-approximated cosmic-shear power spectra formula that neglects an ℓ-dependent factor of

$$T_\ell = \frac{(\ell+2)(\ell+1)\ell(\ell-1)}{(\ell+0.5)^4}, \tag{24}$$

which is equal to unity if the flat-sky approximation is used, and the factor of 0.5 in the denominator is ignored. To include this effect, any Limber-approximated cosmic-shear potential power spectrum $C(\ell)$ should be multiplied by this factor (if not included already).

We investigate how the angular scales in correlation function analyses map on to ℓ modes of the cosmic-shear power spectrum and find that the following scaling relations are a good fit to the behaviour

$$\begin{aligned} \xi_+ &: \log_{10}[\ell_{\rm max}] = -0.14\log_{10}(\theta_{\rm min}/{\rm arcmin}) + 4.06, \\ \xi_- &: \log_{10}[\ell_{\rm max}] = -0.19\log_{10}(\theta_{\rm min}/{\rm arcmin}) + 4.49. \end{aligned} \tag{25}$$

We also present mapping between the various cosmic-shear statistics used in the literature. In translating from the shear power spectrum to configuration statistics such as shear correlation functions, the Hankel transform introduces errors on arcmin scales and higher. A full summation over spherical harmonic modes, using Wigner small-d matrices, is straightforward and preferable.

Many of the approximations we have discussed have relatively small effects, but are unnecessary and there is no good reason to apply them, and for future experiments, such as *Euclid*, LSST and *WFIRST*, which will have very small statistical errors, they should not be applied. Only the Limber approximation may be necessary, and only if computational speed is an issue, and in this case the inaccuracies at low ℓ may be reduced by considering the first two terms in the Limber expansion in LoVerde & Afshordi (2008).

In this paper, we addressed the most prominent approximations; however, there are several further approximations that are expected to have additional impacts on cosmological inference such as source–source clustering (Schneider et al. 2002), source–lens clustering (Bernardeau 1998; Hamana et al. 2002), the Born approximation (Cooray & Hu 2002), higher order power spectrum terms (Krause & Hirata 2010) and the full treatment of unequal-time correlations (Kitching & Heavens 2017).

ACKNOWLEDGEMENTS

TDK is supported by Royal Society University Research Fellowship. RJ and LV acknowledge support by Spanish Mineco grant AYA2014-58747-P and MDM-2014-0369 of ICCUB (Unidad de Excelencia 'Maria de Maeztu' and Royal Society grant IE140357. JDM is supported in part by the Engineering and Physical Sciences Research Council (grant number EP/M011852/1). The Centre for Computational Astrophysics is supported by the Simons Foundation. We thank the creators of CAMB for public release of this code. We thank M. Cropper, H. Hoekstra, A. Lewis and P. Paykari for useful and constructive discussions. We thank C. Wallis for providing the Wigner small-d matrices.

REFERENCES

Albrecht A. et al., 2006, FERMILAB-FN-0793-A, preprint (astro-ph/0609591)
Alsing J., Heavens A., Jaffe A. H., Kiessling A., Wandelt B., Hoffmann T., 2016, MNRAS, 455, 4452
Alsing J., Heavens A., Jaffe A. H., 2017, MNRAS, 466, 3272
Amara A., Réfrégier A., 2008, MNRAS, 391, 228
Bernardeau F., 1998, A&A, 338, 375
Bernardeau F., Bonvin C., Van de Rijt N., Vernizzi F., 2012, Phys. Rev. D, 86, 023001
Bridle S., King L., 2007, New J. Phys., 9, 444
Brown M. L., Taylor A. N., Bacon D. J., Gray M. E. Dye S., Meisenheimer K., Wolf C., 2003, MNRAS, 341, 100

Castro P. G., Heavens A. F., Kitching T. D., 2005, Phys. Rev. D, 72, 023516
Cooray A., Hu W., 2002, ApJ, 574, 19
Cropper M. et al., 2013, MNRAS, 431, 3103
Giannantonio T., Porciani C., Carron J., Amara A., Pillepich A., 2012, MNRAS, 422, 2854
Hamana T., Colombi S. T., Thion A., Devriendt J. E. G. T., Mellier Y., Bernardeau F., 2002, MNRAS, 330, 365
Heavens A. F., 2003, MNRAS, 343, 1327
Heavens A. F., Kitching T. D., Taylor A. N., 2006, MNRAS, 373, 105
Heymans C. et al., 2005, MNRAS, 361, 160
Heymans C. et al., 2012, MNRAS, 427, 146
Heymans C. et al., 2013, MNRAS, 432, 2433
Hikage C., Takada M., Hamana T., Spergel D., 2011, MNRAS, 412, 65
Hildebrandt H. et al., 2017, MNRAS, 465, 1454
Hu W., 1999, ApJ, 522, L21
Hu W., 2000, Phys. Rev. D, 62, 043007
Hu W., White M., 2001, ApJ, 554, 67
Jee M. J., Tyson J. A., Hilbert S., Schneider M. D., Schmidt S., Wittman D., 2016, ApJ, 824, 77
Jeong D., Komatsu E., Jain B., 2009, Phys. Rev. D, 80, 123527
Joachimi B., Bridle S. L., 2010, A&A, 523, A1
Joudaki S., Kaplinghat M., 2012, Phys. Rev. D, 86, 023526
Kaiser N., 1998, ApJ, 498, 26
Kilbinger M., 2015, Rep. Prog. Phys., 78, 086901
Kitching T., Heavens A., 2017, Phys. Rev. D, in press
Kitching T. D., Heavens A. F., Taylor A. N., Brown M. L., Meisenheimer K., Wolf C., Gray M. E., Bacon D. J., 2007, MNRAS, 376, 771
Kitching T. D., Taylor A. N., Heavens A. F., 2008, MNRAS, 389, 173
Kitching T. D., Heavens A. F., Miller L., 2011, MNRAS, 413, 2923
Kitching T. D. et al., 2014, MNRAS, 442, 1326
Köhlinger F., Viola M., Valkenburg W., Joachimi B., Hoekstra H., Kuijken K., 2016, MNRAS, 456, 1508
Krause E., Hirata C. M., 2010, A&A, 523, A28
Kuijken K. et al., 2015, MNRAS, 454, 3500
Laureijs R. et al., 2011, Technical Report ESA/SRE(2011)12, Euclid: Mapping the Geometry of the Dark Universe. European Space Agency
Leistedt B., McEwen J. D., Kitching T. D., Peiris H. V., 2015, Phys. Rev. D, 92, 123010
Limber N., 1953, ApJ, 117, 134
Loverde M., Afshordi N., 2008, Phys. Rev. D, 78, 123506
Massey R. et al., 2013, MNRAS, 429, 661
Munshi D., Valageas P., Barber A. J., 2004, MNRAS, 350, 77
National Research Council, 2010, New Worlds, New Horizons in Astronomy and Astrophysics. National Academies Press
Ng K.-W., Liu G.-C., 1999, Int. J. Mod. Phys. D, 8, 61
Pen U.-L., Van Waerbeke L., Mellier Y., 2002, ApJ, 567, 31
Planck Collaboration I, 2016, A&A, 594, A15
Schneider P., Van Waerbeke L., Mellier Y., 2002, A&A, 389, 729
Schneider P., Eifler T., Krause E., 2010, A&A, 520, A116
Simon P., 2007, A&A, 473, 711
Takada M., Hu W., 2013, Phys. Rev. D, 87, 123504
The DES Collaboration, 2016, Phys. Rev. D, 94, 022001
Tyson J. A., Wittman D. M., Hennawi J. F., Spergel D. N., 2003, Nucl. Phys., 124, 21
Varshalovich D. A., Moskalev A. N., Khersonskiĭ V. K., 1988, Quantum Theory of Angular Momentum. World Scientific Publishing, Singapore

APPENDIX A: SHEAR CORRELATION FUNCTIONS ON THE SPHERE

In this appendix, we derive equation (9), that is, the shear correlation on the celestial sphere. A spin-2 shear field may be written as (see e.g. Hu 2000, appendix A)

$$\gamma_1(\hat{n}) \pm \mathrm{i}\gamma_2(\hat{n}) = \frac{1}{2}\sum_{\ell m}\left[\phi^{\mathrm{R}}_{\ell m} \pm \mathrm{i}\phi^{\mathrm{I}}_{\ell m}\right]\sqrt{\frac{(\ell+2)!}{(\ell-2)!}}\,{}_{\pm 2}Y^{m}_{\ell}(\hat{n}), \tag{A1}$$

where $\phi_{\ell m}$ is the spherical harmonic transform of the lensing potential with real and imaginary components, ${}_{\pm 2}Y^{m}_{\ell}(\hat{n})$ are spin-2 spherical harmonics and $\hat{n}$ are angular celestial coordinates. The shear power spectrum is related to the lensing potential power spectrum by

$$\begin{aligned} C^{\mathrm{E},\gamma\gamma}_{\ell} &= \frac{1}{4}\frac{(\ell+2)!}{(\ell-2)!}C^{\phi^{\mathrm{R}}\phi^{\mathrm{R}}}_{\ell}, \\ C^{\mathrm{B},\gamma\gamma}_{\ell} &= \frac{1}{4}\frac{(\ell+2)!}{(\ell-2)!}C^{\phi^{\mathrm{I}}\phi^{\mathrm{I}}}_{\ell}, \end{aligned} \tag{A2}$$

that is, the E and B modes are related to correlations of the real and imaginary parts of the lensing potential. To compute ξ_+, it is easiest to consider two points that are at the same azimuthal angle, separated by an angle in the polar direction. In this case, $\xi_+ = \langle(\gamma_1+\mathrm{i}\gamma_2)(\gamma_1+\mathrm{i}\gamma_2)^*\rangle = \langle\gamma_1(\hat{n})\gamma_1(\hat{n}')\rangle + \langle\gamma_2(\hat{n})\gamma_2(\hat{n}')\rangle$ and $\xi_- = \langle(\gamma_1+\mathrm{i}\gamma_2)(\gamma_1-\mathrm{i}\gamma_2)^*\rangle = \langle\gamma_1(\hat{n})\gamma_1(\hat{n}')\rangle - \langle\gamma_2(\hat{n})\gamma_2(\hat{n}')\rangle$, with $\hat{n}$ and $\hat{n}'$ separated by β, and

$$\begin{aligned} \xi_+(\beta) &= \langle(\gamma_1+\mathrm{i}\gamma_2)(\gamma_1+\mathrm{i}\gamma_2)^*\rangle = \frac{1}{4}\sum_{\ell m\ell' m'}\left(\left\langle\phi^{\mathrm{R}}_{\ell m}\phi^{\mathrm{R}}_{\ell' m'}\right\rangle + \left\langle\phi^{\mathrm{I}}_{\ell m}\phi^{\mathrm{I}}_{\ell' m'}\right\rangle\right)\frac{(\ell+2)!}{(\ell-2)!}\,{}_2Y^{m}_{\ell}(\hat{n})\,{}_2Y^{m'*}_{\ell'}(\hat{n}') \\ &= \frac{1}{4}\sum_{\ell m}\left[C^{\phi^{\mathrm{R}}\phi^{\mathrm{R}}}_{\ell} + C^{\phi^{\mathrm{I}}\phi^{\mathrm{I}}}_{\ell}\right]\frac{(\ell+2)!}{(\ell-2)!}\sum_{m}\,{}_2Y^{m}_{\ell}(\hat{n})\,{}_2Y^{m*}_{\ell}(\hat{n}') = \sum_{\ell}\left[C^{\mathrm{E},\gamma\gamma}_{\ell} + C^{\mathrm{B},\gamma\gamma}_{\ell}\right]\sqrt{\frac{2\ell+1}{4\pi}}\,{}_2Y^{-2}_{\ell}(\beta,0), \end{aligned} \tag{A3}$$

where the last inequality comes from (equation 7; with $\alpha = \tilde{\gamma} = 0$; note that, $\tilde{\gamma}$ here refers to an Euler angle not shear, but we use this as it is standard notation):

$$\sum_{m}\,{}_2Y^{m}_{\ell}(\hat{n})\,{}_2Y^{m*}_{\ell}(\hat{n}') = \sqrt{\frac{2\ell+1}{4\pi}}\,{}_2Y^{-2}_{\ell}(\beta,0). \tag{A4}$$

In terms of Wigner-D matrices,

$$D^{\ell}{}_{-ms}(\alpha,\beta,-\tilde{\gamma}) = (-1)^{m}\sqrt{\frac{4\pi}{2\ell+1}}\,{}_sY^{m}_{\ell}(\beta,\alpha)\mathrm{e}^{\mathrm{i}s\tilde{\gamma}}, \tag{A5}$$

hence

$$\xi_+(\beta) = \sum_\ell \left(\frac{2\ell+1}{4\pi}\right)\left[C_\ell^{\mathrm{E},\gamma\gamma} + C_\ell^{\mathrm{B},\gamma\gamma}\right] D_{22}^\ell(0,\beta,0), \tag{A6}$$

or in a more compact form in terms of small-d Wigner matrices

$$\xi_+(\beta) = \frac{1}{2\pi}\sum_\ell (\ell+0.5) d_{22}^\ell(\beta)\left[C_\ell^{\mathrm{E},\gamma\gamma} + C_\ell^{\mathrm{B},\gamma\gamma}\right]. \tag{A7}$$

A similar calculation for $\xi_-(\beta)$ is trivial by replacing the $+$ with $-$ in the derivation corresponding to the other case in equation (A1). These results can also be derived trivially from Ng & Liu (1999) equations (4.5)– (4.8) by identifying CMB polarization quantities with their shear analogues.

APPENDIX B: THE EXTENDED LIMBER APPROXIMATION FOR COSMIC SHEAR

In LoVerde & Afshordi (2008), an extended Limber approximation is presented that was used to assess the accuracy of this approximation as a function of ℓ mode. Their main result can be captured in the following approximation

$$\lim_{\epsilon\to 0}\int_0^\infty \mathrm{e}^{-\epsilon(x-\nu)} f(x) J_\nu(x)\mathrm{d}x = f(\nu) - \frac{1}{2}f''(\nu) - \frac{\nu}{6}f'''(\nu) + \ldots, \tag{B1}$$

where $\nu = \ell + 1/2$, $J_\nu(x)$ are Bessel functions (not spherical) and $f(x)$ is some arbitrary function. Dashes denote derivatives with respect to x. This is then applied to the case of a non-evolving matter power spectrum $P(k)$ (LoVerde & Afshordi 2008; equation 5) and an extended Limber approximation computed (LoVerde & Afshordi 2008; equation 11). This calculation however is not strictly appropriate for the cosmic shear case because the matter power spectrum is an evolving field $P(k, z)$.

For cosmic shear, we start with equation (5)

$$U_\ell(r[z], k) = \int_0^{r[z]} \mathrm{d}r' \frac{F_K(r, r')}{a(r')} j_\ell(kr') P^{1/2}(k, r'), \tag{B2}$$

which describes the kernel function for the spherical-Bessel and spherical-radial representations of the cosmic shear field. The integral is along a line of sight to a source redshift plane $r[z]$ and encodes the radial transform of the integrated lensing effect caused by perturbations in the matter over-density, that are mapped to the power spectrum via Poissons equation. To make this into a form for which the LoVerde & Afshordi (2008) expansion can be applied, we rewrite this as

$$U_\ell(r[z], k) = \int_0^\infty \mathrm{d}r' w(r[z], r') \frac{F_K(r, r')}{a(r')} j_\ell(kr') P^{1/2}(k, r'), \tag{B3}$$

where $w(r, r')$ is a weight function with the following properties: $w(r, r') = 1$ for $r' \leq r$ and $w(r, r') = 0$ for $r' > r$. We can now apply the Limber approximation and find that to first order

$$U_\ell^{\mathrm{L}}(r[z], k) = \left(\frac{\pi}{2\nu k^2}\right)^{1/2} w(r[z], \nu/k) \times \frac{F_K(r, \nu/k)}{a(\nu/k)} P^{1/2}(k, \nu/k) + \ldots, \tag{B4}$$

where $\nu = \ell + 1/2$; and the pre-factor is a result of the conversion from a spherical-Bessel function to a Bessel function. It can be seen explicitly that the weight function is now $w(r, \nu/k) = 1$ for $\nu/k \leq r$, and $w(r, \nu/k) = 0$ for $\nu/k > r$.

The expansion of this case to higher orders can be done using equation (B1); however, it can be seen that the calculation is more complex than the LoVerde & Afshordi (2008) derivation because the function $f(x)$ in that equation is now $f(r'|r, k) = (\pi/2k^3r)^{1/2} w(r[z], r')[F_K(r, r')/a(r')]P^{1/2}(k, r')$. In particular, the expansion does not affect the weight function evaluation $w(r, \nu/k)$ because the arguments to this do not change in the higher order terms. Also, the expansion is only valid over the region $\nu/k < r$, where the derivatives of this function are not divergent.

We can now attempt to derive the standard weak-lensing formulation of the Limber-approximated cosmic shear power spectrum (Kaiser 1998) using equations (7) and (8). Substituting equation (B4), we find that

$$C_\ell^{\mathrm{SR,L}}(z_i, z_j) = |D_\ell|^2 \mathcal{A}^2 \left(\frac{2}{\pi}\right) \int \frac{\mathrm{d}k}{k^2} \int \mathrm{d}z_\mathrm{p}\mathrm{d}z'\mathrm{d}z'_\mathrm{p}\mathrm{d}z'' n(z_\mathrm{p}) n(z'_\mathrm{p}) \times p(z'|z_\mathrm{p}) p(z''|z'_\mathrm{p}) W^{\mathrm{SR}}(z_i, z_\mathrm{p}) W^{\mathrm{SR}}(z_j, z'_\mathrm{p}) \left(\frac{\pi}{2\nu k^2}\right)$$
$$\times \frac{F(r(z'), \nu/k)}{a(\nu/k)} \frac{F(r(z''), \nu/k)}{a(\nu/k)} P(k, \nu/k), \tag{B5}$$

where we have absorbed the weight functions w into the integral limits for clarity, and $\mathcal{A} = 3\Omega_\mathrm{M} H_0^2/(2c^2)$. To express this equation in the standard form, we need to transform integration variables from k to r in the outer integral. This leads to

$$C_\ell^{\mathrm{SR,L}}(z_i, z_j) = |D_\ell|^2 \mathcal{A}^2 \left(\frac{1}{\nu^4}\right) \int \mathrm{d}r r^2 \int \mathrm{d}z_\mathrm{p}\mathrm{d}z'\mathrm{d}z'_\mathrm{p}\mathrm{d}z'' n(z_\mathrm{p}) n(z'_\mathrm{p}) \times p(z'|z_\mathrm{p}) p(z''|z'_\mathrm{p}) W^{\mathrm{SR}}(z_i, z_\mathrm{p}) W^{\mathrm{SR}}(z_j, z'_\mathrm{p})$$
$$\times \frac{F(r(z'), r)}{a(r)} \frac{F(r(z''), r)}{a(r)} P(\nu/r, r); \tag{B6}$$

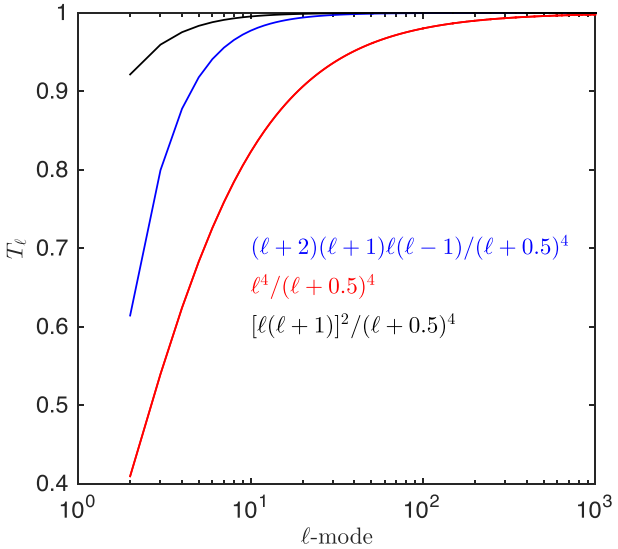

Figure B1. The functional form of the ℓ-dependent pre-factor in equations (B8), (B9) and (B10), for the cosmic shear spherical (blue) and flat-sky (red) cases, and for the convergence case (black).

the inner integrals can now be expressed in terms of kernel functions

$$q(r_i, r) = \frac{r}{a(r)} \int \mathrm{d}z_\mathrm{p} \mathrm{d}z' n(z_\mathrm{p}) p(z'|z_\mathrm{p}) W^\mathrm{SR}(z_i, z_\mathrm{p}) \left(\frac{r(z') - r}{r(z')} \right), \tag{B7}$$

where we have expanded the function F_K for the flat-geometry case ($K = 0$), where the Limber-approximated power spectrum can be written as

$$C_\ell^{\mathrm{SR,L}}(z_i, z_j) = |D_\ell|^2 \mathcal{A}^2 \left(\frac{1}{\nu^4} \right) \int \mathrm{d}r \frac{q(r_i, r) q(r_j, r)}{r^2} P(\nu/r, r). \tag{B8}$$

This is the standard form for the cosmic shear power spectrum (see e.g. Hu 1999; Joachimi & Bridle 2010), except that the ℓ-dependent pre-factor is different. The full ℓ mode dependent pre-factor is

$$T_\ell = \frac{|D_\ell|^2}{\nu^4} = \frac{(\ell+2)(\ell+1)\ell(\ell-1)}{(\ell+0.5)^4}. \tag{B9}$$

In the standard derivation, there are two assumptions that remove this pre-factor. These assumptions are the flat-sky approximation whereby $|D_\ell|^2 = \ell^4$, and the approximation $\nu = \ell$ (or $\ell = (\ell + 0.5)$). In this case, $T_\ell = 1$ and the standard result is recovered. However, these approximations can have a large impact on the amplitude of the power spectrum at $\ell \lesssim 100$ as we investigate in this paper.

In Fig. B1, we show the functional form of T_ℓ. To recover the correct ℓ mode scaling from a standard cosmic shear analysis one should multiply by T_ℓ.

One can also compute a convergence power spectrum from weak-lensing data. This is different from the shear case only in that the factor $D_\ell = \ell(\ell + 1)$ in the spherical-sky case. Following the derivation above, we find that the Limber-approximated convergence power spectrum is the same as equation (B8) but with an ℓ-dependent pre-factor of

$$T_\ell^\kappa = \frac{[\ell(\ell+1)]^2}{(\ell+0.5)^4}. \tag{B10}$$

Again, under the assumption that $\nu = \ell$ and $\ell \simeq \ell + 1$ this factor cancels, but does not in general as also noted by Joudaki & Kaplinghat (2012). We again show the effect in Fig. B1, which is less pronounced than for the shear case.

This paper has been typeset from a TEX/LATEX file prepared by the author.